Numerical Investigation of Roof Stability in Longwall Face Developed in Shallow Depth under Weak Geological Conditions

Mao, Pisith
Key Laboratory of Deep Coal Resource Mining (CUMT), Ministry of Education of China, School of Mines, China University of Mining and Technology

Hashikawa, Hiroto
Laboratory of Rock Engineering and Mining Machinery, Department of Earth Resources Engineering, Kyushu University

Sasaoka, Takashi
Laboratory of Rock Engineering and Mining Machinery, Department of Earth Resources Engineering, Kyushu University

Shimada, Hideki
Laboratory of Rock Engineering and Mining Machinery, Department of Earth Resources Engineering, Kyushu University

他

出版情報：sustainability. 14 (3), pp.1036-, 2022-01-18. Multidisciplinary Digital Publishing Institute : MDPI
バージョン：

sustainability

MDPI

Article

Numerical Investigation of Roof Stability in Longwall Face Developed in Shallow Depth under Weak Geological Conditions

Pisith Mao [1,2,3], Hiroto Hashikawa [2], Takashi Sasaoka [2,*], Hideki Shimada [2], Zhijun Wan [1,*], Akihiro Hamanaka [2] and Jiro Oya [4]

1 Key Laboratory of Deep Coal Resource Mining (CUMT), Ministry of Education of China, School of Mines, China University of Mining and Technology, Xuzhou 221116, China; maopisith@cumt.edu.cn
2 Laboratory of Rock Engineering and Mining Machinery, Department of Earth Resources Engineering, Kyushu University, Fukuoka 819-0395, Japan; hashikawa20r@mine.kyushu-u.ac.jp (H.H.); shimada@mine.kyushu-u.ac.jp (H.S.); hamanaka@mine.kyushu-u.ac.jp (A.H.)
3 Materials Science and Structure Unit, Research and Innovation Center, Institute of Technology of Cambodia, Phnom Penh 12150, Cambodia
4 Business Planning Department, Mitsui Matsushima Holdings Co., Ltd., Fukuoka 810-8527, Japan; j-oya@mitsui-matsushima.co.jp
* Correspondence: sasaoka@mine.kyushu-u.ac.jp (T.S.); zhjwan@cumt.edu.cn (Z.W.)

Abstract: Developing longwall mining under weak geological conditions imposes a substantial challenge with regard to the higher risk of falling roofs. Maintaining the stability of the longwall face in this aforementioned condition is crucial for smooth operation. Investigating roof conditions in longwall requires detailed study of rock behavior in response to a few key influences. This paper presents the outcome of a numerical analysis of roof stability in shallow depth longwall face under weak geological conditions. A series of validated FLAC3D models was developed to examine the roof condition of the longwall face under the influence of shield canopy ratio, shield resistance force, and stress ratio. The results show that these three key factors have a significant impact on longwall roof conditions, which can be used to optimize its stability. Two distinct mechanisms of the roof caving behavior can be observed under the influence of stress ratio. The countermeasures of reducing face-to-tip distance and cutting width are proposed to improve the roof condition of longwall face under weak rock. The outcomes show a substantial improvement in roof conditions after adopting the proposed method.

Keywords: numerical analysis; weak geological conditions; shallow depth; longwall face; roof stability; shield configurations

Citation: Mao, P.; Hashikawa, H.; Sasaoka, T.; Shimada, H.; Wan, Z.; Hamanaka, A.; Oya, J. Numerical Investigation of Roof Stability in Longwall Face Developed in Shallow Depth under Weak Geological Conditions. *Sustainability* **2022**, *14*, 1036. https://doi.org/10.3390/su14031036

Academic Editor: Guang-Liang Feng

Received: 29 December 2021
Accepted: 13 January 2022
Published: 18 January 2022

1. Introduction

Global energy consumption is projected to increase in the next decade [1,2]. Coal consumption is still considered the main player in the energy sector, although it is usually associated with emission problems [3,4]. Coal production is mainly mined using longwall mining methods since this method provides high resource recovery. The stability of the longwall face is one of the fundamental considerations when it comes to designing a sustainable longwall mine [5,6]. The face of the longwall is the region where the coal seam is excavated. The stability of the longwall face is fully maintained by the array set of powered shield support. Although the advanced longwall system has been improved with the automated system, it always required some miners to work in the longwall face to keep the extraction operation running. Inappropriate selection of powered shield support can lead to potential incidences, including roof falls, floor heave, and face collapse, which will disrupt coal production or even lead to fatalities [7]. The investigation on longwall face stability provides the impact of safety and prevent disaster in a sustainable coal resources development.

Since the early introduction of the Longwall mining method, face stability has usually been the center of attention for many researchers from the introduction of conventional face support to semi-automated systems and fully automated systems. Recent research by Ji et al. [8] has used the superposition technique to study the behavior and failure mechanism of the overlying roof strata generating their failure pattern and mechanical state. The result indicated that yield degree and yield distance were the main controllers on the roof failure which could occur in front of the longwall face or over goaf area. An experimental study by Tian et al. [9] on the fracture and deformation of the working coal face by considering non-uniform bearing pressure area shows that the coal wall goes through a complex fracturing phenomenon which is directly linked to distance from the coal face. Most of the surface fracture in coal face is tensile, while shear or combination between the two can be found further away from the face. Other researchers have studied shield support interaction with the overlying roof strata by performing model tests on various types of shield support which results in different fracture zone under different strength parameters of rock [10]. Others have used numerical simulations to estimate and predict the behavior of surrounding rock in a longwall face, the interaction of roof with powered shield support, stability of the coal pillar, and influence of dynamic pressure in longwall mining with substantial outcomes [10–16].

There are two characteristics of the powered shield support, namely its load resistance capacity, which is usually provided by one or two pairs of high-pressure legs, as well as the position of the legs, which can lead to a different resistance stress distribution depending on the canopy ratio [17]. The correct static balance conditions of the powered shield support are significantly influenced by canopy ratio, which results in a reduction in the stress distribution that occurs between the coal face and roof [11]. According to previous research, there is a wide range of shield resistance forces adopted for research studies, which ranges from 2000 up to 260,000 kN depending on the characteristics of the studied longwall mine site [12,13,18]. Witek and Prusek [19] simulated the behavior of shield support stress with different load-bearing capacities and load distributions. Their outcome specified that the stress value of the shield base depends on the canopy loading pattern and is the highest when the load condition is asymmetrical and the lowest when the load is applied to the entire surface of the canopy.

Weak geological conditions have proven to impose many challenges in the development of longwall mining [20–22]. The lack of rock strength competence requires its own investigation of its rock mass, strata behavior, stress distribution, deformation, and exclusive support design during mine development and operation [21–25]. A big portion of the global coal reserves is located in weak geological conditions [26–29]. Specifically, for Indonesia, which is one of the world's largest coal reserve countries, most of its coal reserves are usually found in weak rock zones [30–33]. In addition to rock mechanical properties, the surrounding stress conditions also have a major influence on longwall development in weak rock. For instance, a change in horizontal stress can result in entry gate roof failure in the form of cutter and sagging, especially for weak roof geology in shallow depth [34]. There is not a universal definition of what depth is considered shallow for longwall mining. It usually depends on the country and its relative average depth of the mine. However, studies of shallow depth longwall mine are usually located at a depth up to 400 m [35,36]. The changing stress induced by the redistribution of load can also cause a large deformation surrounding the working area [37].

Review of previous research demonstrates that the appropriate selection of shield support and accurate prediction of roof caving behavior are the two crucial influences of face stability, which can directly be linked to many factors such as mechanical properties of coal and surrounding rocks, shield configurations, in situ stress, etc. Previous studies seldom considered shallow and weak geological conditions in the research work, as their study field is often located in deep and hard rock conditions. It is doubtful that those studies can be applied to coal field located in weak geological conditions. Research on the stability of longwall face in weak geological conditions is very limited. The strata

behavior of the rock under weak geological conditions deserves a detailed investigation, as it could turn out to be entirely different from that of hard rock, especially for longwall mining, a method that is able to completely exploit the coal reserve. Although longwall development has already been carried out for many decades, the uniqueness of the new site study still captivated innovative study aspects, method of analysis, issue consideration for mining optimization, and sustainability. For this study, in particular, we focus on developing longwall under weak geological conditions by considering several local key issues by means of numerical analysis. There are several other ways of studying longwall development including empirical analysis, field monitoring, and physical modeling. Due to the complexity of each site condition, a numerical analysis is usually considered to be the main tool for the analysis because of its overall flexibility and scale. However, the drawback of this method is that it still requires some field monitoring data for validating analysis accuracy as well as some empirical estimation for the unavailable parameters. As a result, a series of numerical models is established to investigate the interaction between shield support and roof strata under weak geological conditions by considering different types of shield resistance force distribution, shield capacity, and stress conditions. Based on the validated numerical models, the interaction between shield support and weak roof strata can be investigated in detail and a countermeasure for controlling face stability is proposed which can be adopted in a relevant longwall mining project or be useful for future research work.

2. Studied Site

This research is carried out on the Kutai Basin of East Kalimantan province, the second-largest coalfield in Indonesia. The total coal resource in this province is estimated to be around 37,904 Mt [38]. The studied site is situated near Samarinda town. The geological structure of the coal seam in the studied area is dominated by a monocline structure with a maximum dip angle of up to 13°. The depth of the mineable coal seam can reach 300 m. The stratigraphy of this area is associated with two formations known as Balikpapan Formation and Pulau Balang Formation, which formed during the middle to upper Miocene [39]. Coal seams in this area are surrounded by weak claystone with a maximum uniaxial strength around 13 MPa on average for the studied depth up to 300 m. Claystone is considered the dominant rock in this area. According to laboratory tests, the strength of the dominant rock is correlated with depth. Due to the lack of available initial stress information, initial vertical stress and horizontal stress are estimated using Equations (1) and (2) as follows [40].

$$\sigma_v = \sum_{i=1}^{n} \gamma_i g H_i \quad (1)$$

$$\sigma_h = k\sigma_v \quad (2)$$

where σ_v is vertical stress, σ_h is horizontal stress, γ is rock density, g is gravity constant and H is the thickness of rock strata.

Figure 1 displays the general mine layout of the studied area. The mine layout is composed of two incline entries, namely the north slope and the south slope, which are connected to the two main entries. The entry size is 5 m in width by 3 m in height. The entry roof is supported by a 1 m spacing of steel arches with a maximum yield strength of 540 MPa. A parallel series of mine panels is formed by a 121 longwall system, which consists of one working face, two entries, and one protective chain pillar in between the mining panel. The panel configuration is 130 m in width and 500 m to 1000 m in length with 30 m width of coal pillar between the panel.

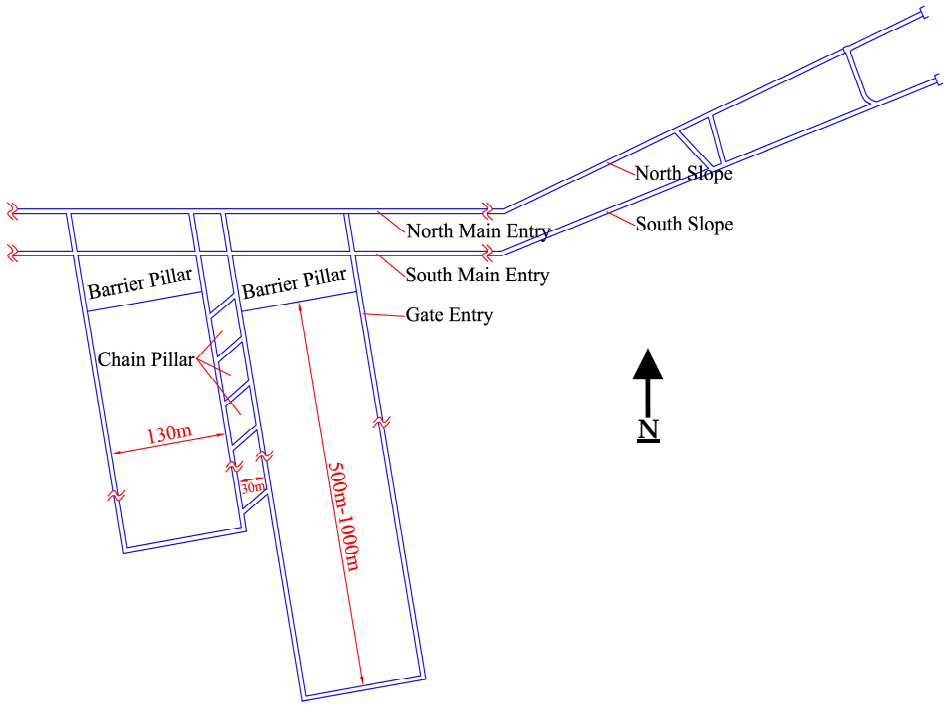

Figure 1. General mine layout of the studied area.

3. Establishment of Numerical Model

3.1. Global Model Description

The three-dimension models are constructed and analyzed in FLAC3D (Fast Lagrangian Analysis of Continua in Three-Dimensions) based on the actual onsite conditions. The longwall panel configurations for modeling include the panel width of 130 m, chain pillar width of 30 m as well as 5 m by 3 m of gate cross-section which is supported by 1 m spacing of steel arch. The overall dimension for the global model is shown in Figure 2a. Following the symmetry principle in numerical modeling, the model consists of two half-widths of longwall panels, which are separated by two gate entries and a chain pillar in between. The total dimension of the model is 170 m × 100 m × 78 m (Length × Width × Height). A 3-m coal seam is modeled in between the dominant rock claystone. In the global model, the claystone thickness is 50 m and 25 m for overburden and underburden, respectively. To obtain highly accurate simulation results, the mesh size surrounding the longwall face is densified as shown in Figure 2b. The mesh size of the densified zone is 0.25 m. The base of the model is fixed in all three translation directions. Horizontal compression stress is applied on the four sides of the model based on the initial in-situ horizontal stress condition of the case study. Compression vertical stress is applied on top of the model to simulate in-situ vertical stress generated according to the cover depth at which the coal seam is located. Stress ratio K, which is the ratio of horizontal stress to vertical stress, is used to represent initial stress conditions for the study. The range of stress ratio is vary based on the location. Generally, for 300 m depth, it is around 0.5 to 2 [23–25,41]. For the studied site, the range of stress ratio is assumed to be from 0.5 to 2. The constitutive model for the numerical simulation is based on the Mohr-Coulomb failure criterion. The laboratory results of core samples from the actual site indicate that the strength of the claystone is depth-dependent. The strength of claystone increases with increasing depth. For that reason, four types of claystone properties are adopted for the simulation for the cover depth of 50 m, 100 m, 200 m, and 300 m. Table 1 lists all rock properties used in this research, while Table 2 shows the mechanical properties of the steel beam used for simulating support structural elements. Steel beam configurations in Figure 2c is adopted for gates roof support. This steel beam is called SS540 which provides maximum yield strength of around 540 MPa.

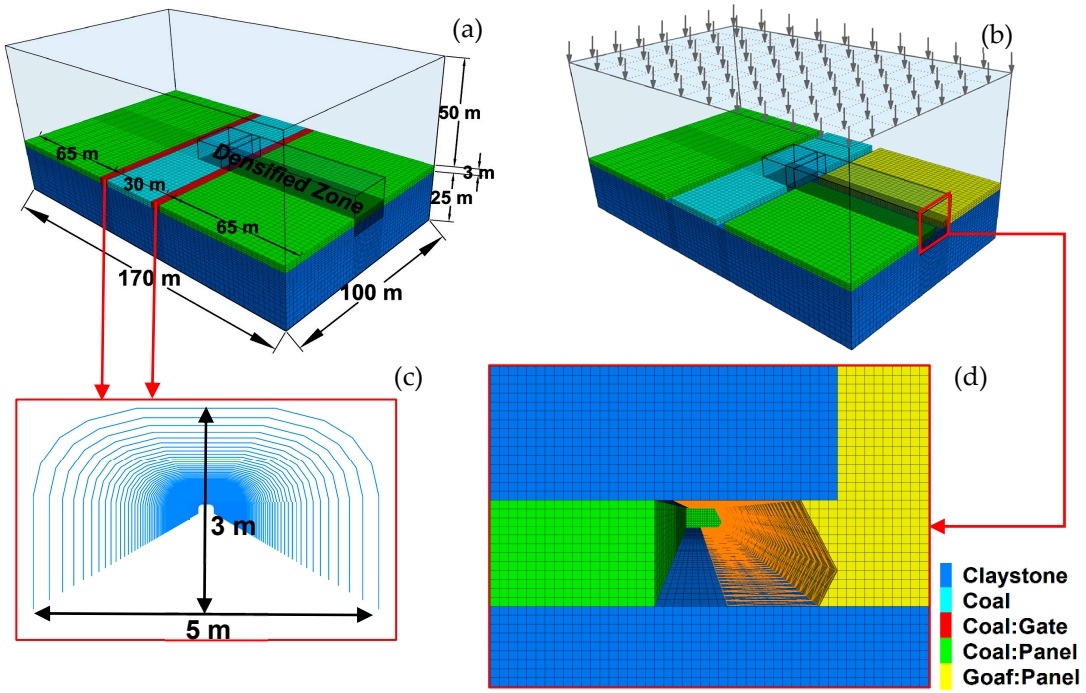

Figure 2. Global model: (**a**) model dimension, (**b**) model after panel excavation, (**c**) steel beam, (**d**) longwall face.

Table 1. Summary of rock properties used in the simulation.

Rock	Compressive Strength (MPa)	Density (kg/m^3)	Young's Modulus (MPa)	Poisson's Ratio	Cohesion (MPa)	Internal Friction Angle (°)	Tensile Strength (MPa)
Claystone (50 m)	2.72	2095	268	0.28	0.14	33.08	0.38
Claystone (100 m)	4.84	2110	800	0.28	0.60	37.45	0.52
Claystone (200 m)	9.08	2140	1880	0.28	1.07	46.18	0.80
Claystone (300 m)	13.32	2160	2960	0.28	1.54	54.91	1.08
Coal	8.16	1380	1300	0.32	2.63	45.60	0.58
Goaf	-	1700	15	0.25	0.001	25	-

Table 2. Summary of steel beam properties using in the simulation.

Density (kg/m^3)	Young's Modulus (GPa)	Poisson's Ratio	Cross-Sectional Area (cm^2)	Maximum Yield Strength (MPa)	Second Moment Y-Axis (m^4)	Second Moment Z-Axis (m^4)	Polar Moment of Inertia (m^4)
7800	200	0.3	36.5	540	732×10^{-8}	154×10^{-8}	22×10^{-8}

Figure 2b also demonstrates the model state at the end of the simulation process. The modeling steps consist of: (1) constructing the model geometry and mesh; (2) analyzing for the initial state; (3) excavating and installing support to the gates; (4) retreating the longwall panel for 50 m. A detailed illustration of the longwall face can be found in Figure 2d. The longwall face is supported by powered shield support. The detail of goaf modeling is explained by Sasaoka, et al. [25]. Since roof caving occurs in the goaf area which makes the whole area inaccessible, it is very difficult to study and obtain goaf behavior. Most of the research investigates goaf using the indirect method. Goaf properties are estimated using trial and error. For this study, goaf properties are adopted from the previous research.

During panel retreat, the excavated rock zone properties and roof caving zone are switched to goaf properties. Caved zone height can be determined by Equation (3) as follows [42,43]:

$$h_c = \frac{100h_m}{c_1 h_m + c_2} \tag{3}$$

where h_c is caved zone height, h_m is the working thickness, and c_1 and c_2 are the strata strength coefficients, whose values can be identified according to Table 3. Since the maximum compressive strength of rock is 13.32 MPa and the working thickness is 3 m, the caving zone can be calculated to be 5.92 m.

Table 3. Strata strength coefficient.

Strata Strength	Compressive Strength (MPa)	Coefficient	
		c_1	c_2
Hard Rock	>40	2.1	16
Medium-hard Rock	20–40	4.7	19
Weak Rock	<20	6.2	32

There are two stability indicators in this study, failure zone, and shield displacement. Failure zone is an area zone where the stresses fulfill the yield criterion. The mechanism of failure can occur in shear mode and tension mode [44]. This can indicate a possible roof fall, face collapse, and floor heave in the longwall face. For instance, an illustration of the failure zone from the simulation result in a 300-m depth case is presented in Figure 3a where "None" legend represents the non-failure zone and other legends represent the mode of failure. Although the ultimate goal is to maintain the stability of the longwall face, it is impossible to completely diminish the failure zone in the face during longwall operation. Thus, it is required to consider the allowable range of fracture control, above which the failure zone is exceeded, to consider that the roof is in poor condition. Zhao et al. [12] adopted 0.4 m as the allowable range for roof control. Due to the mesh size in this study, 0.5 m is adopted for this study as the allowable range of roof control. If the failure zone exceeds the 0.5 m range, the rock is considered in poor condition.

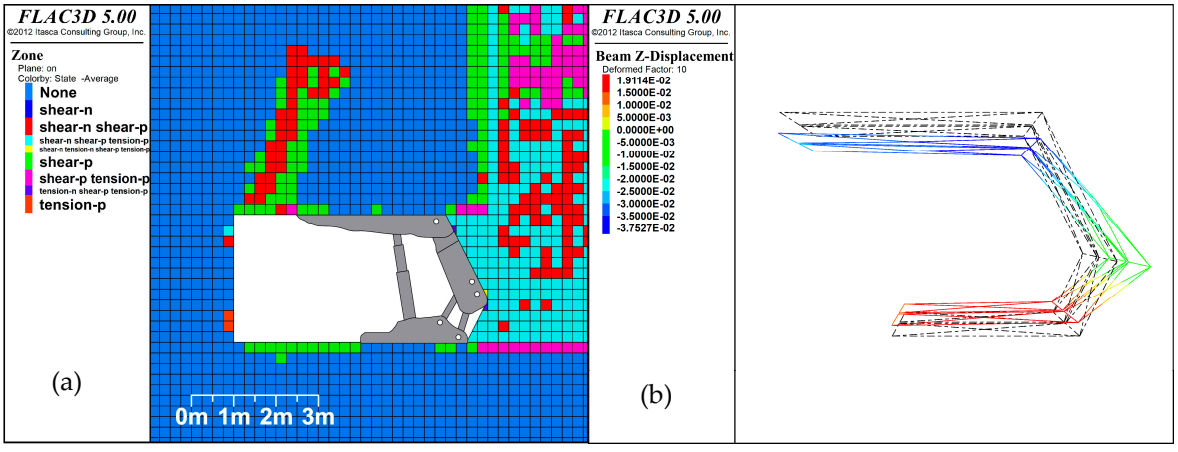

Figure 3. Stability indicators: (**a**) failure zone result, (**b**) shield vertical convergence result.

Total shield convergence is also a good indicator of shield selection. A review of several modern support designs confirmed that set-to-yield convergence is about 1.1 to 1.5 mm per 1MPa pressure [45]. Cheng and Peng [46] monitored the set-to-yield convergence of the shield support in a mine site and indicated that the maximum initial set-to-yield convergence is 12 mm during the load cycle. Set-to-yield convergence is one of the shield support specifications and is commonly provided with the technical specification of the

support. When exceeding the specification set-to-yield convergent rate, it can lead to the reduction of support stiffness, hence poor roof condition. The simulating result specimen of the vertical convergence of the shield support is shown in Figure 3b.

3.2. Simulation Model of Powered Shield Support

In this study, the two-leg powered shield support is selected. Powered shield support is the most essential component for maintaining the stability of the longwall face to make panel retreat possible. The component of shield support comprises the canopy, the base, back-shield plate, and hydraulic legs. The working mechanism of the shield support is mainly based on the resistant power of the hydraulic legs. The canopy and base plate of the shield support interact directly with the working face overlying roof and floor. Figure 4a illustrates the typical interaction of shield support with the surrounding rock in the longwall face. The position of the leg is essential in determining the interaction behavior between the shield and the surrounding rock [10]. The different position of the legs results in different resistant stress distribution of the canopy and the base of the shield. The calculation of shield canopy ratio (CR) can be found in Figure 4a. Canopy ratio is the ratio of leg-to-tip distance to leg-to-back distance of the canopy. For model simulation, the shield plate is modeled using a series of interconnected beams, a type of structural element function in FLAC3D linked together to create a shield plate structure, as shown in Figure 4b. The dynamic pressure change of the hydraulic leg cannot be simulated using any type of structural element available in FLAC3D. As a result, the resistance stress of the shield leg is simulated using the applied boundary stress on the canopy and the base of the shield support as shown in Figure 4b. The distribution of applied boundary stress is based on the canopy ratio of shield support. As shown in Figure 5, due to the width of the longwall shearer head, it is impossible that the tip of the canopy reach the longwall face. For the initial state before the cutting (before web), there is already a distance between the longwall face to the tip of the canopy due to the length of the shearer. After the cutting (after web), this distance increases depending on the cutting width. Typically, the distance from the longwall face to tip of the canopy is 0.5 m and the web width is 1 m.

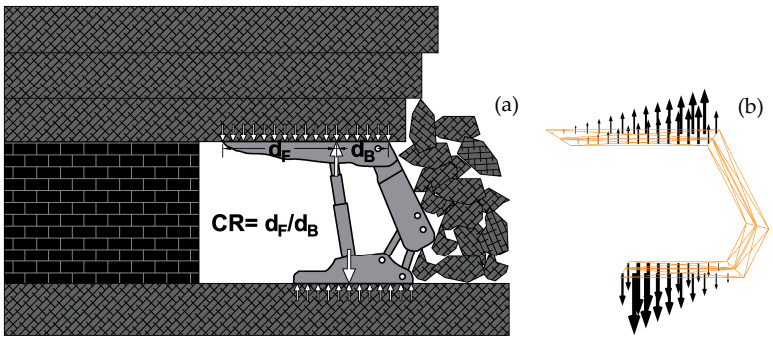

Figure 4. Shield support: (**a**) Interaction between shield support and surrounding rock, (**b**) Modelling of shield support.

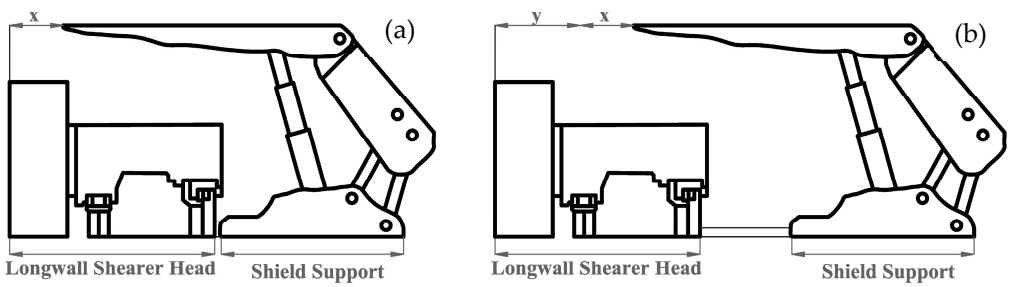

Figure 5. Cross-section of longwall machineries: (**a**) before web, (**b**) after web [x: face-to-tip distance, y: cutting width].

3.3. Research Scheme

The initial parameters for all analysis conditions include a canopy ratio of 2, shield resistance force of 10,000 kN, and stress ratio of 1 for the three depths of the coal seam cases, which are 100 m, 200 m, and 300 m. Parametric studies include varieties of shield canopy ratios, shield resistance forces, and stress ratios as described below.

- Canopy ratios are CR2, CR2.5, and CR3.2.
- Shield resistance forces are 6000 kN, 8000 kN, 10,000 kN, 12,000 kN
- Stress ratios K are 0.5, 1, 1.5, and 2

Throughout the analysis of one parametric study condition, the others two parameters are set to initial values. For instance, the shield resistance force and stress ratio are kept in initial value when investigating the influence of the canopy ratio.

All types of shied support have the same canopy length of 3.5 m and base plate length of 2.5 m, shield width of 2 m, and working height of 3 m. The different component of each shield variation is the location of the leg, which results in different canopy ratios and hence different shield resistant stress distribution. The detailed stress distribution of the shield support with different canopy ratios are shown in Figure 6. For the case where the canopy ratio is 2, the position of the leg is at the one-third length of the canopy from the back of the plate, resulting in a triangular distribution of resistance stress on the canopy plate. The ideal leg position at the base for this case is one-third length of the base from the front of the base, which results in a reverse triangular distribution, compared to the canopy. As shown in Figure 6, when the canopy ratio increases, the leg position becomes closer to the back of the canopy. As the leg position is close to the back of the canopy, the distribution of resistance stress is concentrated in the back portion of the canopy leaving the front portion of the canopy without any resistance stress. The leg position at the base also moves toward the center of the base when the canopy ratio increases. This can cause the resistance stress distribution at the base to become a trapezoidal shape when the leg moves close to the center, or a rectangular shape when the leg is at the center of the base. Table 4 demonstrates the conversion value of the different leg resistance forces to the applied boundary stress for each type of shield support. These values are obtained by converting the resistance force of the shield legs to the surface resistance stress according to the distribution shape of the resistance stress for each canopy ratio shown in Figure 6. For CR2 as an example, the resistance force of 6000 kN is distributed the force to 3.5 m × 2 m plate of the canopy. Since the distributed load is known to be triangular distribution, the highest point of this triangular distributed load 'A' is equal to 6000 kN/(3.5 m × 2 m) × 2 which is equal to 1.71 MPa.

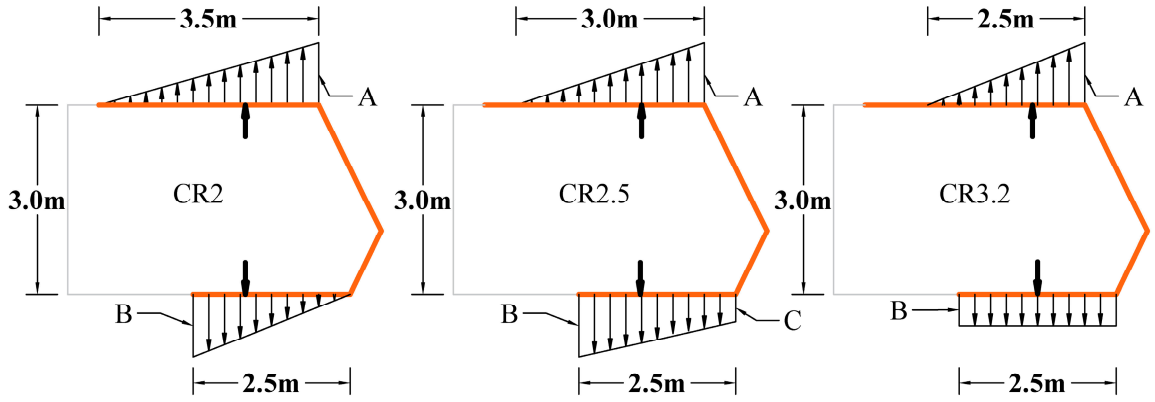

Figure 6. Applied stress boundary distribution of each canopy ratio (A, B, and C: applied stress value).

Table 4. Apply boundary stress converting from shield resistance force.

Shield Resistance Force (kN)	Applied Stress (MPa)					
	CR2		CR2.5		CR3.2	
	Canopy	Base	Canopy	Base	Canopy	Base
6000	A = 1.71	B = 2.40	A = 2.00	B = 2.40 C = 0.50	A = 2.40	B = 1.20
8000	A = 2.28	B = 3.20	A = 2.66	B = 2.53 C = 0.66	A = 3.20	B = 1.60
10,000	A = 2.85	B = 4.00	A = 3.33	B = 3.16 C = 0.83	A = 4.00	B = 2.00
12,000	A = 3.42	B = 4.80	A = 4.00	B = 3.80 C = 1.00	A = 4.80	B = 2.40

3.4. Model Validation

Model validation is a crucial step for numerical investigation to evaluate the legitimacy of the modeling process in representing the actual case study. Field measurement data of the selected field study are quite limited due to its early stage of mine development. There are no field measurement data from the actual longwall face to validate the powered shield since longwall panel extraction has not been yet started. However, there are a couple of field measurements available that can be utilized for model validation. During the main gate development, the roof displacement is monitored using two different types of devices, namely telltale and extensometer. These results are useful for validating the model in this study. Another valuable field measuring data is surface subsidence from the nearby mine which is available from the previous research publication. After assessing the location, rock properties, and geological conditions in that mine, it is found that the overall field conditions are comparable to those of the selected study area. As a result, these available field monitoring results are used for the validation of the model in this study.

3.4.1. Roadway Roof Displacement

The installation of telltale and extensometer on the roof of the main gate provided a vital roof displacement for validating the model. Telltale 28 and Extensometer 35 are selected for model validation due to their similar condition in terms of cover depth with the overburden thickness of the global model which is 50 m. The actual cover depth of these devices is 45 m. Therefore, the overburden of the model is adjusted to 45 m to accurately simulate the actual conditions for model validation with the assumption that the initial stress ratio is 1. Telltale is used to monitor the displacement on the roof. The extensometer, on the other hand, can record roof movement or displacement from 0.3 m to 6 m above the roof with the interval of the anchor point of 0.3 m. However, the obtained results from the extensometer from anchor point 0.3 m to 1.2 m display a highly fluctuating value which could result from a large fracture on the roof which possibly affects the anchor point within this range. As a result, roof displacement result from this device is monitored at 1.5 m above the roof. The results of roof displacement from the numerical simulation are measured at two points. The first point is on the roof and the second point is 1.5 m above the roof. These results are compared with the recorded data from the aforementioned devices. The compared result is shown in Figure 7. Since the evolution of roof displacement in the simulation process is based on the simulation step, there is no suitable method to convert these simulation steps to the actual time frame to compare with the field monitoring data which is recorded in the specific time frame. However, this simulation result is meant to illustrate the static snapshot of the model during its equilibrium state. Likewise, the evolution of roof displacement in field measurement devices will be stationary when it reaches an equilibrium state. According to Figure 7, the evolution of roof displacement in the simulation reaches the maximum value of 17.3 mm on the roof and 12.2 mm at 1.5 m

above the roof, which are in great agreement with the field monitoring results from both devices whose values are 17 mm and 11.5 mm, respectively.

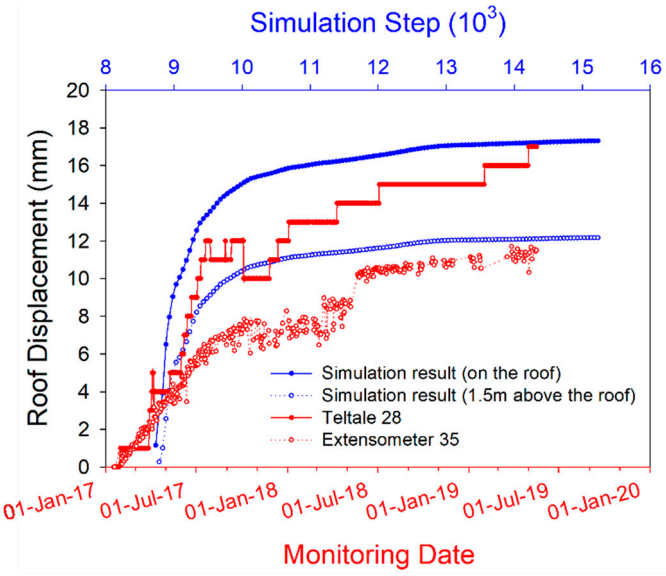

Figure 7. Roof displacement comparison between simulation and field measurement.

3.4.2. Surface Subsidence

In the study of surface subsidence by Sasaoka, et al. [20] which is located near the study area, surface displacement is monitored during longwall operation. The monitoring stations are arranged into two lines, namely line 1 and line 2, above the operated longwall panel. Line 2 is selected for a validated simulation model due to its resemblance of cover depth around 50 m. The panel width of the global model is adjusted to fit the actual panel width of 80 m in the compared study. However, the working thickness cannot be adjusted to fit the 2 m of the compared study as it will affect the overall model mesh, shield configuration, and interaction between the shield support and rock surrounding the longwall face which could result in an inconsistent analysis result in the global model. Thus, the working thickness is kept at 3 m. There are three surface movement monitoring stations located along line 2, which begin from the middle of the working panel. Longwall face had been retreated approximately 100 m before reaching monitoring line 2. The field result is recorded when the longwall face passed line 2 roughly 2.8 m. In the modeling, the panel retreats for 100 m length after which the surface displacement is exported from the 97 m length which is 3 m behind the longwall face. The compared result is illustrated in Figure 8. The maximum surface subsidence in the middle of the panel from the simulation is slightly higher than the actual field measurement. It is to be expected since the working thickness of the simulation is thicker than the actual field. However, the overall trend of the surface displacement profile is still consistent between the simulated and measured results. This confirms the validity and usability of the numerical model proposed for this study.

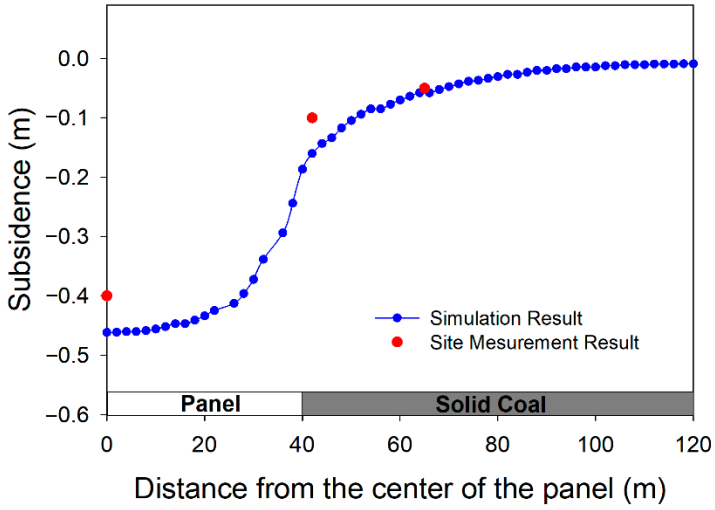

Figure 8. Surface subsidence comparison between simulation and field measurement.

4. Results and Discussion

The outcome of this research utilizes numerical simulation to predict the failure zone and shield convergence for different depths under the influence of several parameters including canopy ratio of shield support, shield resistance force as well as stress ratio. Since the properties of rock change according to the depth of longwall excavation, the result of the stability analysis of the longwall face is divided into three different depths. These results are further separated into before web, where face-to-tip distance is 0.5 m, and after web, where the face-to-tip distance is 1.5 m. The results of these investigations are presented in Tables 5–12 and Figures 9–12.

4.1. Effect of Shield Support Canopy Ratio on Stability of Longwall Face

4.1.1. Failure Zone Surrounding Longwall Face

There are three types of canopy ratios presented in the previous section. Table 5 shows the results for longwall face stability under the effect of different shield types before web. During this stage, the only visible difference in the efficiency of each type of shield in terms of maintaining the stability of the longwall is shown in the depth of 100 m where the roof has the lowest strength. The vertical failure zone for all canopy ratio is 0.5 m. However, the CR2 has the smallest horizontal failure zone. Because CR2 provides well-distributed resistance stress on the canopy, it allows the whole canopy length to act as the support, hence a better support efficiency. For depths of 200 m and 300 m, it is relatively stable in this stage. However, a small increase in the propagation of the horizontal failure zone can be seen with the change of support from CR2 to CR3.2.

The cutting web extended failure zone which can further indicate the correlation between the failure zone and the canopy ratio of the shield support (Table 6). During this stage, the influence of the shield canopy ratio can be observed up to a 200-m depth, where the strength of the roof is considered moderate. For a 100-m depth, the vertical failure zone increases from 1 m to 1.75 m when the canopy ratio increases. Combining with a wider extent of horizontal fracture in CR2.5 and CR3.2 results in a larger area of the failure zone. As a result, the CR2 shield provides the best result in terms of keeping the roof relatively more stable. In between the adoption of these three variations of shield support canopy ratio for 200 m, the vertical failure zone is not significantly different. However, horizontal failure zones of CR2.5 and CR3.2 are extended more compared to the case of CR2, which also suggests that CR2 is the better choice for shield support. For 300-m depth, in which the roof is relatively harder, there is no significant difference in the failure area between those shield types. The result of this section demonstrates that CR2 is the most efficient

support, especially when it comes to the weaker rock in the shallower depth. The influence of canopy ratio becomes insignificant for the harder roof.

Table 5. Failure zone under the influence of canopy ratio (before web).

Depth	Canopy Ratio: CR		
	2.0	**2.5**	**3.2**
100 m	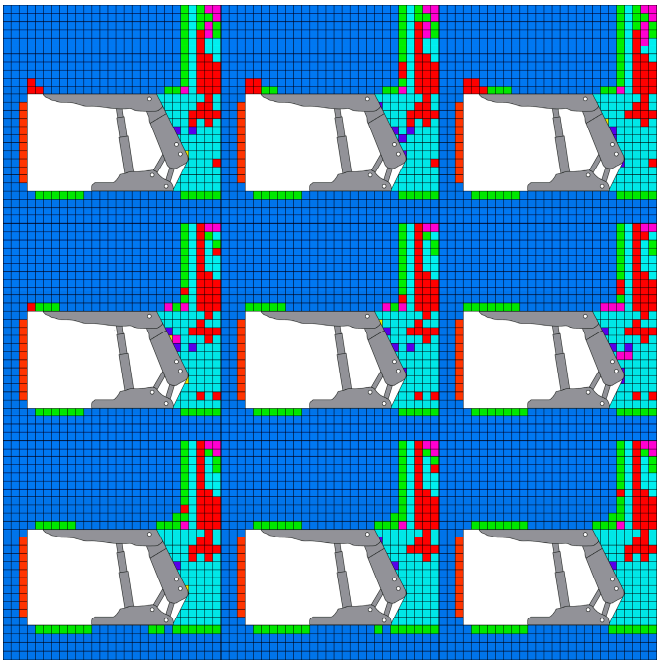		
200 m			
300 m			

Table 6. Failure zone under the influence of canopy ratio (after web).

Depth	Canopy Ratio: CR		
	2.0	**2.5**	**3.2**
100 m	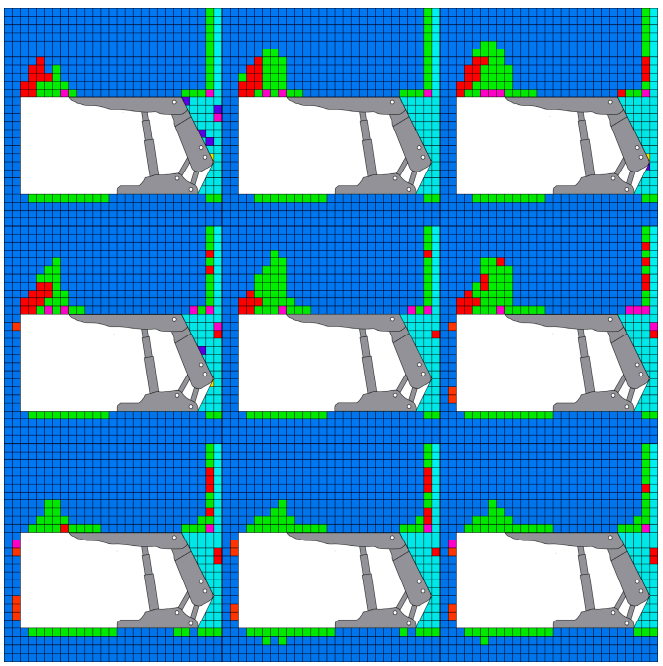		
200 m			
300 m			

4.1.2. Shield Convergence

Figure 9 shows the shield convergence under the different shield canopy ratios. The canopy ratio has no effect on shield convergence. The explanation for this behavior can be seen in the displacement contour shown in Figure 3b. The maximum vertical displacement is located in the end part of the canopy where the resistance stress of the shield support is at the maximum value. Thus, the change in canopy ratio will not have any substantial effect on shield convergence as the studied canopy ratio will only influence the tip and the front part of the canopy. The maximum shield convergence range is 30 mm to 45 mm which is comparable to the outcome from the research work of Zhao et al. [12] where the range is around 20 mm to 35 mm. The smaller shield convergence of this study is due to the higher roof strength. The bar chart represents the increment percent of convergence during shield loading after web in comparison to the convergence before web. The results show the increase of shield convergence of 100%, 80%, and 65% on average for a depth of 100 m, 200 m, and 300 m, respectively. Since the roof condition of the shallower depth is relatively weak, cutting web can cause the roof to develop more fractures which result in a higher impact on shield convergence.

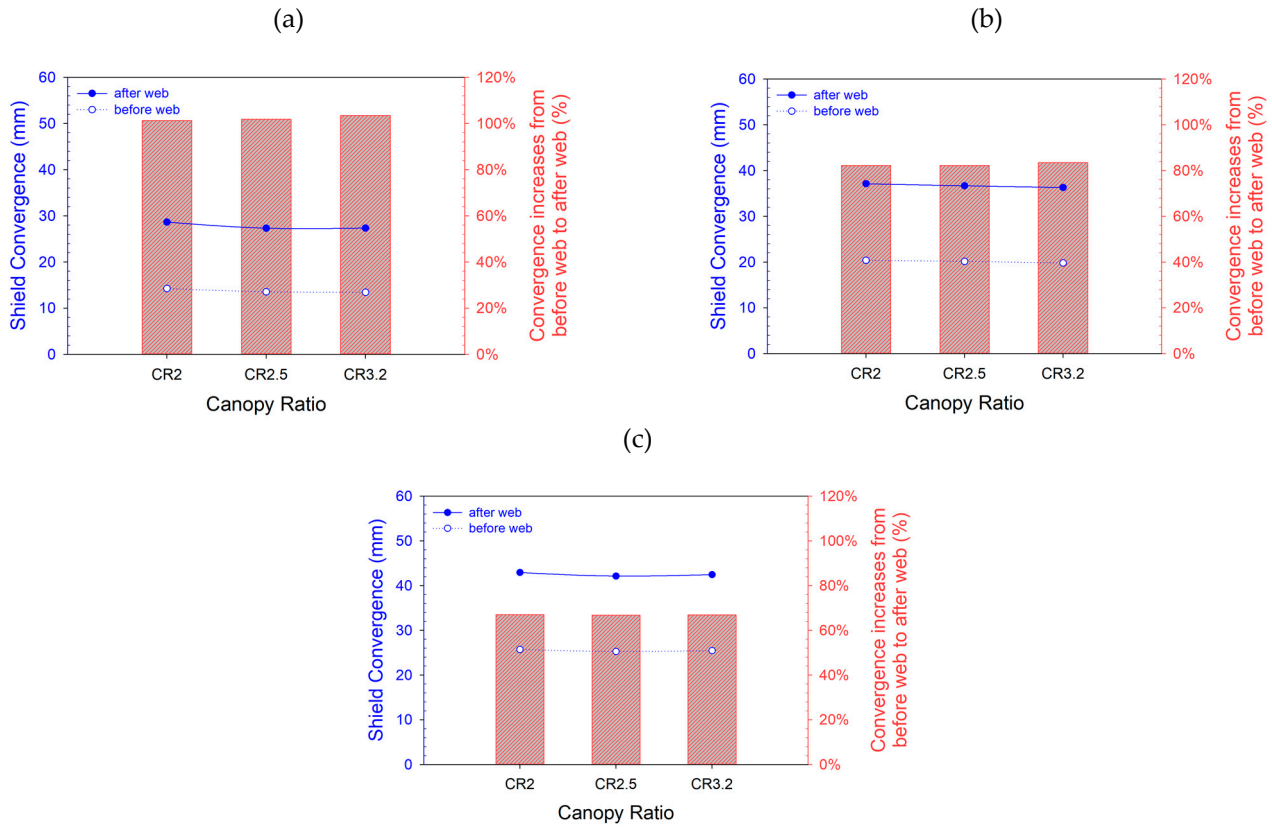

Figure 9. Shield convergence under the influence of canopy ratio: (**a**) 100 m, (**b**) 200 m, (**c**) 300 m.

4.2. Effect of Shield Resistance Force on Stability of Longwall Face

4.2.1. Failure Zone Surrounding Longwall Face

In longwall mining, shield support goes through the loading cycle during each retreating step for the longwall face. Shield resistance force is set at a certain value during the stage before web which is also known as setting pressure. After web, the roof above the shield begins to collapse, which results in more loading acting on the shield. This phenomenon causes the pressure of the shield to increase at a certain time. In the case of none yield condition, the pressure of the shield is released and retreated and begin the cycle again. The result of the stability of the longwall face with the influence of shield resistance capacity before web is presented in Table 7. This result can represent the resistance force

at the beginning of the loading cycle. Resistance force in this stage represents the setting pressure. According to these results, the longwall face is relatively stable for all depths. Even in 100-m depth cases, where the rock strength is relatively low, the vertical failure zone penetrates 0.5 m regardless of the resistance force adopted. With the increasing resistance force from 6000 kN to 8000 kN in 100 m depth, the failure zone of the roof only has a slight improvement. Above 8000 kN, there is no change in terms of the failure zone. These results show that the influence of the setting pressure is very minimal on the stability of the longwall face during this stage. Setting pressure can be set as low as 6000 kN as the failure zone is still in the allowable range of roof control.

Table 7. Failure zone under the influence of shield resistance force (before web).

Depth	Shield Resistance Force (kN)			
	6000	8000	10,000	12,000
100 m	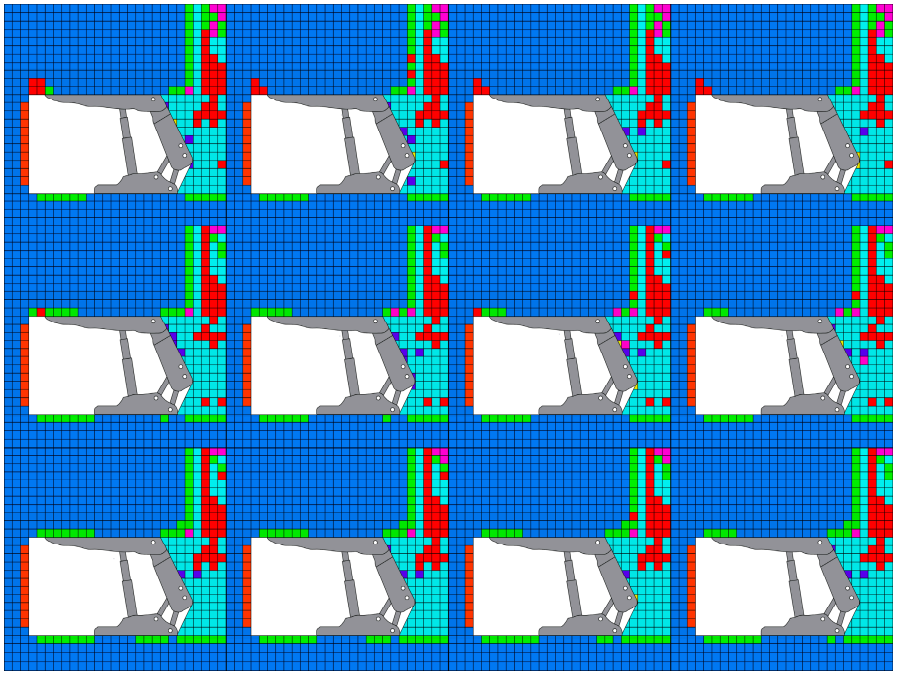			
200 m				
300 m				

Table 8 illustrates the failure zone of the longwall face after web with different resistance forces. This resistance force can represent the maximum pressure before the shield is released and retreating in non-yield conditions. The result shows that these pressures have an effect on maintaining the stability of the longwall face. For both 100-m and 200-m depth cases, a significant decrease of the vertical failure zone can be observed when the resistance force increases from 6000 kN to 12,000 kN. However, the change is very small in case of a depth of 300 m which shows only a settle effect of the resistance force for this depth. Due to the strength of the roof in 300-m depth being stronger than the shallower depth, it required less shield resistance force. It can be said that shield resistance force can reduce the failure zone on the roof. A higher shield resistance force is required for the shallow depth due to its weaker roof condition.

Table 8. Failure zone under the influence of shield resistance force (after web).

Depth	Shield Resistance Force (kN)			
	6000	8000	10,000	12,000
100 m	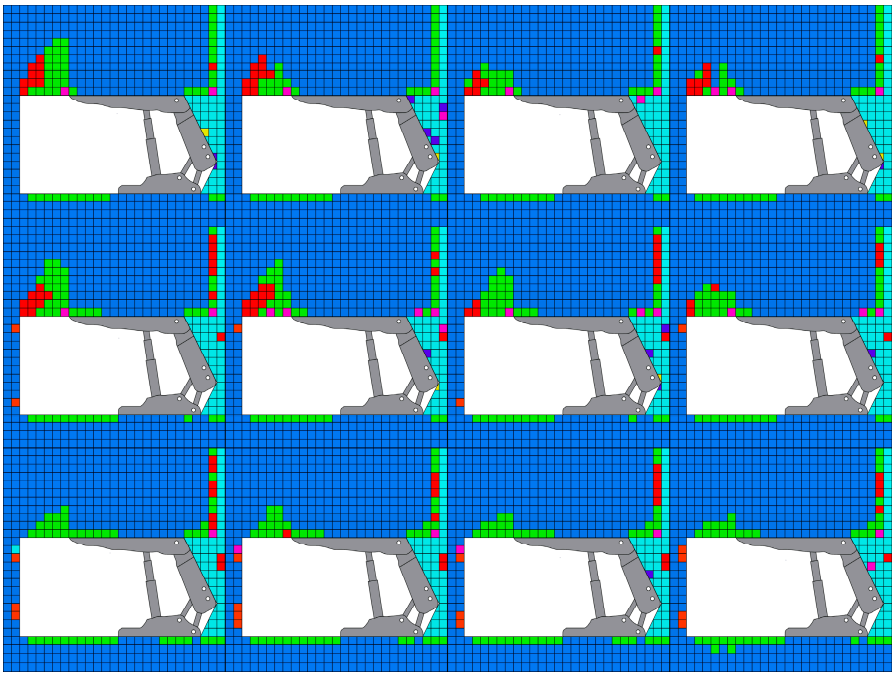			
200 m				
300 m				

4.2.2. Shield Convergence

The results of shield convergence under different resistance forces are presented in Figure 10. The average increment percentage of convergence between before and after web for each depth is also 98%, 80%, and 65% for the respective depths. The maximum convergence for 6000 kN cases reaches 33 mm, 40 mm, and 45 mm for the respected depth of 100 m, 200 m, and 300 m after web. When resistance force increases, the convergence decreases at a rate of 8%, 4%, and 2% for the respective depth. The result points out that resistance force has a slight effect on the convergence of the longwall face. The effect seems even less significant for the deeper depth of 300 m.

(a) (b)

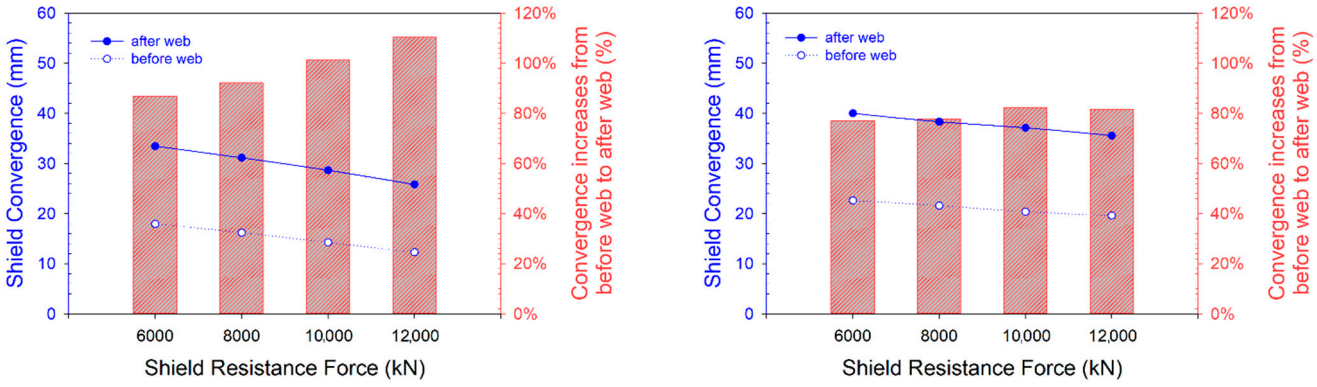

Figure 10. *Cont.*

(c)

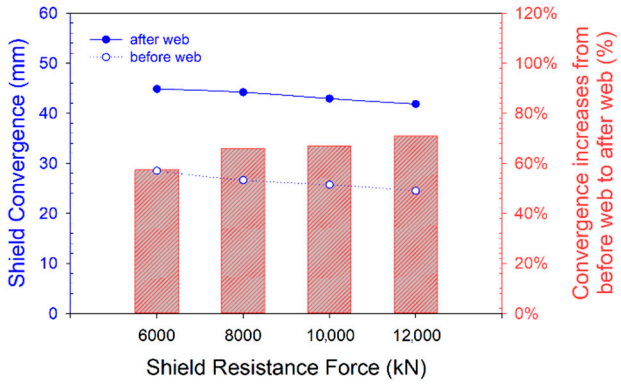

Figure 10. Shield convergence under the influence of shield resistance force: (**a**) 100 m, (**b**) 200 m, (**c**) 300 m.

4.3. Effect of Stress Ratio on Stability of the Longwall Face

4.3.1. Failure Zone Surrounding Longwall Face

The result of longwall face stability before web under the influence of stress ratio is shown in Table 9. These results indicate that before web, the longwall face is relatively stable in most of the studied stress ratios. Except for cases of low stress ratio in shallower depths of 100 m and 200 m where the roof failure zone is 0.5 m, the failure zone is penetrated at only a 0.25 m distance for the roof, the floor, and coal face. The combination of low stress ratio of 0.5 and low strength roof in 100 m depth product a longer range of vertical failure zone up to 0.75 m on the roof. According to Table 9, for low stress ratio, roof failure zone tends to develop vertically. In contrast, the high stress ratio develops the roof failure zone in a horizontal direction.

Table 10 represents the failure zone developed after web. Due to the cutting web, the failure zone significantly extended, which better illustrates the effect of the stress ratio on the stability of the longwall face. These outcomes indicate that the orientation of roof failure is based on the condition of stress ratio. The results at a stress ratio of 0.5 have shown a large failure zone develops vertically above the roof. This fracture is very large and the failure zone in 100 m and 200 m cases are propagated to the caved zone in the goaf area. This can generate a highly dangerous condition for the longwall face to develop a potential roof fall. Due to the higher strength of the roof at depth 300 m, the fracture is also significant but not propagated into the caved zone, which makes it less dangerous than the two previous depths. From these results, in the area where stress ratio is 0.5, roof fall is expected, especially in the shallow depth panel. For all depths, the failure zone in the vertical direction is decreased when the stress ratio increases. However, at stress ratio 2, the failure zone begins to expand in both horizontal and vertical directions. As seen in Table 10, for a 200-m depth, the vertical range of the failure zone decreases from 1.75 m at a stress ratio of 1 to 0.5 m at stress ratio of 1.5. However, when the stress ratio further increases to 2, the vertical range of the failure zone also increases. The apparent lack of continuity can be explained by the wider range of the horizontal failure zone, which could also promote the vertical failure zone. Hence, for the stress ratio of 2 and above, the overall failure zone will start to increase again. The most stable stress condition for the longwall mine in this region should fall into the range of stress ratio higher than 1 but lower than 2. Table 10 also shows that the potential of the buckling effect on the face area also increases when the stress ratio increases for 300 m depth. This buckling is caused by the increase in horizontal stress. Even in the condition of a small failure zone on the roof, the buckling effect can increase the risk of danger by initiating the failure zone to propagate from the roof to the coal face especially in a deeper area with a higher stress ratio. However, according to this result, up to stress ratio 2, the buckling effect is still in a manageable condition. The solution to this longwall

face stability problem with a low stress ratio of 0.5 can be improved by adopting an incline timber pile roof reinforcement method to improve roof conditions.

Table 9. Failure zone under the influence of stress ratio (before web).

Depth	Stress Ratio: K			
	0.5	**1**	**1.5**	**2**
100 m	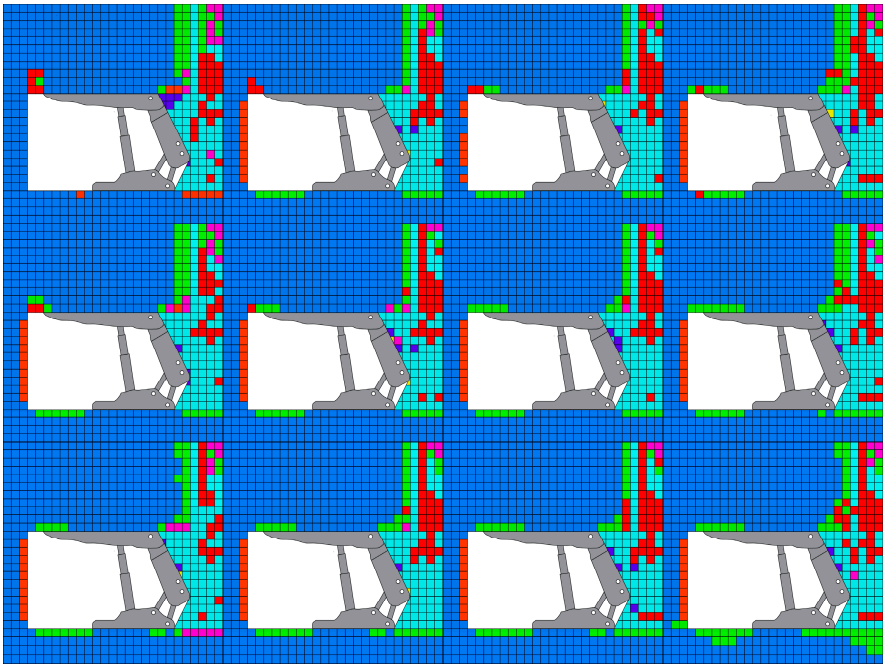			
200 m				
300 m				

These results also allow us to understand the mechanism of the roof caving behavior of the longwall face. At a lower stress ratio of 0.5 where the horizontal stress is less than vertical stress, the behavior of the roof caving follows the detached block model. The mechanism behind this behavior is that the higher intensity of vertical stress will affect the roof to move downward. Since there is not enough horizontal stress to counteract with vertical stress, the failure zone is moving upward and connecting to the caved zone which easily detaches when the shield supports move forward. As the stress ratio increases above 1, the horizontal stress also increases. As a result, a higher support effect from the horizontal stress on the roof is available to counteract the intensity of the vertical stress. This leads the roof caving mechanism to behave differently more towards the bending mechanism. This behavior follows the bulking model, which according to Galvin [47], considers shield support as a displacement control system.

4.3.2. Shield Convergence

The results of the shield convergence under the influence of different stress ratios are illustrated in Figure 11a–c. The results lend support to the idea that the stability of longwall stress is more stable with a higher stress ratio. For all depth cases, before web, the convergence is at their maximum value in stress ratio of 0.5 which are 19 mm, 28 mm, and 34 mm for 100 m, 200 m, and 300 m depth, respectively. Through all the case studies, when the stress ratio increases from 0.5 to 2, the values of the convergence decrease in the average rate of 23%, 26%, and 22% for the respective depths. This statement is also true for the case after web. By comparing the convergence between before and after web, the convergence increases in the average rate of 100% for 100 m depth, 75% for 200 m depth, and 60% for 300 m depth which lead the maximum shield convergence to 37 mm, 50 mm and 57 mm for the respective depths.

Table 10. Failure zone under the influence of stress ratio (after web).

Depth	Stress Ratio: K			
	0.5	**1**	**1.5**	**2**
100 m	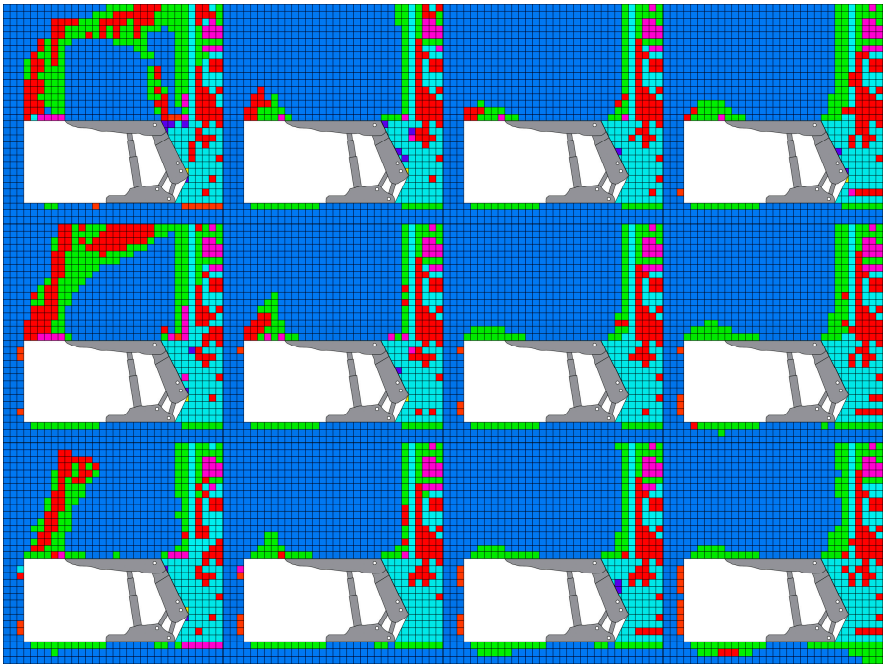			
200 m				
300 m				

(a) (b)

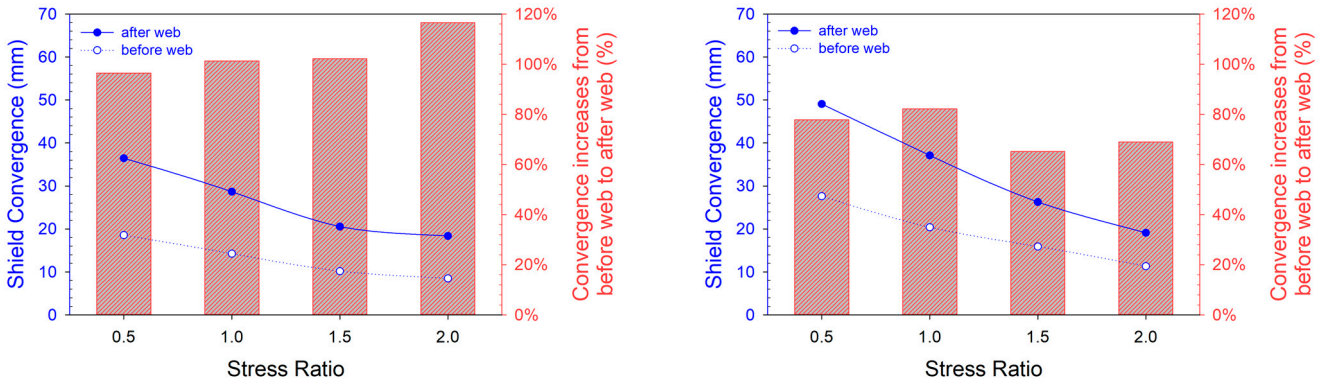

(c)

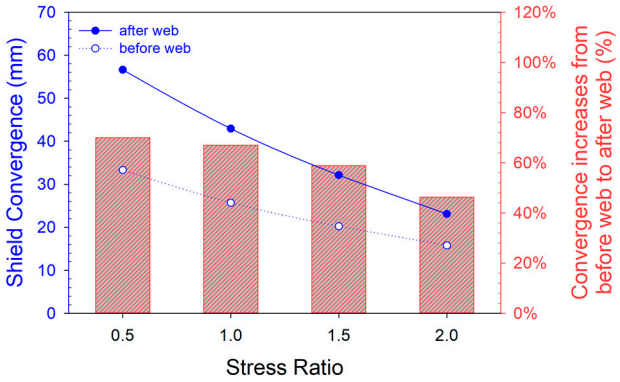

Figure 11. Shield convergence under the influence of stress ratio: (**a**) 100 m, (**b**) 200 m, (**c**) 300 m.

5. Stability Control of Longwall Face Stability under the Weak Geological Conditions

The stability of the longwall face can be optimized according to the outcomes and discussion from the previous section. However, even though the best available option of the case study such as canopy ratio 2, high shield resistance force of 12,000 kN is not able to minimize the roof failure zone to the allowable range of stability control in the longwall face stability study which is around 0.5 m. In the typical coal mine, optimizing the parameters above should improve the stability of the longwall face to the allowable range. However, because the studied area is located in weak geological conditions, optimizing these parameters is not enough to keep the face in stable condition. As a result, a guideline for countermeasures is needed to further improve the stability of the longwall face. One of the proposed strategies is to modify the cutting configuration which has a smaller face-to-tip distance before web and to reduce the cutting width of the web. To demonstrate the effectiveness of this strategy, the numerical model is configured to reduce the aforementioned distance. In this case, the adoption of the face-to-tip distance of the canopy is 0.25 m. The web width is reduced to 0.5 m. Shield with canopy ratio 2 and resistance force of 10,000 kN is adopted as the base case study for this. The drawback of this strategy is that it will affect the overall time of the panel advancing operation.

Table 11 shows the result of the failure zone before web when the suggested countermeasure is adopted. The results indicates that the adopted method have reduced the failure zone of all case studies before web below the allowable range of 0.5 m. This shows the effectiveness of the proposed method. On the other hand, Table 12 shows the result after web. According to these results, the suggested method is also really effective for stress ratios of 1 and above. A significant improvement in terms of the stability of the longwall face can be observed when compared to Table 10. However, for the stress ratio of 0.5, even adopted the suggested countermeasure method, the risk of roof fall still remains very high. Great attention has to be paid to the longwall face located in the shallow depth with low stress ratio. The roof reinforcement method is a must for operating longwall face extraction under these ground conditions. The recommended roof reinforcement is the utilization of incline timber piles or wooden bolts as it would not interfere with the shear cutter.

Table 11. Failure zone after adopting the countermeasure (before web).

Depth	Stress Ratio: K			
	0.5	**1**	**1.5**	**2**
100 m	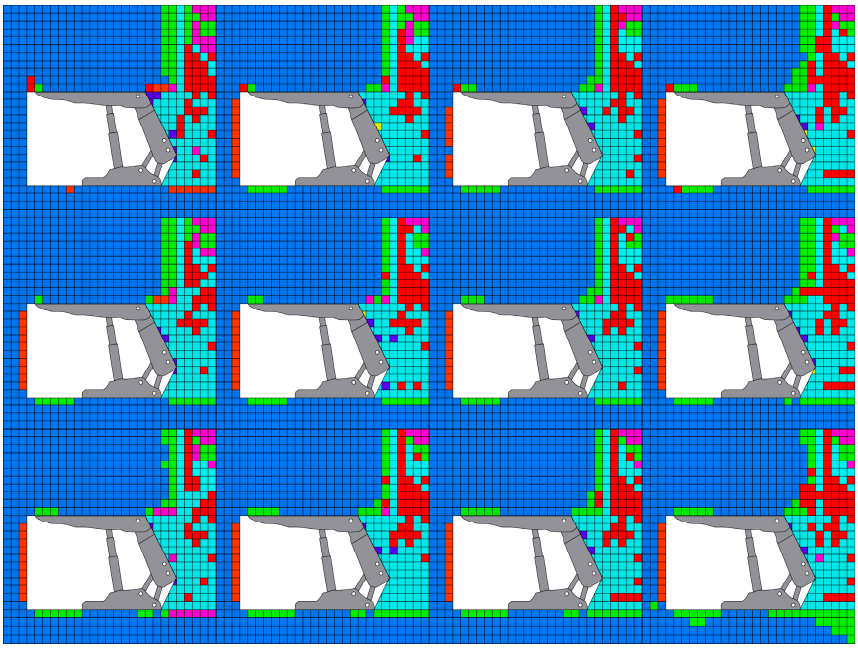			
200 m				
300 m				

Table 12. Failure zone after adopting the countermeasure (after web).

Depth	Stress Ratio: K			
	0.5	**1**	**1.5**	**2**
100 m	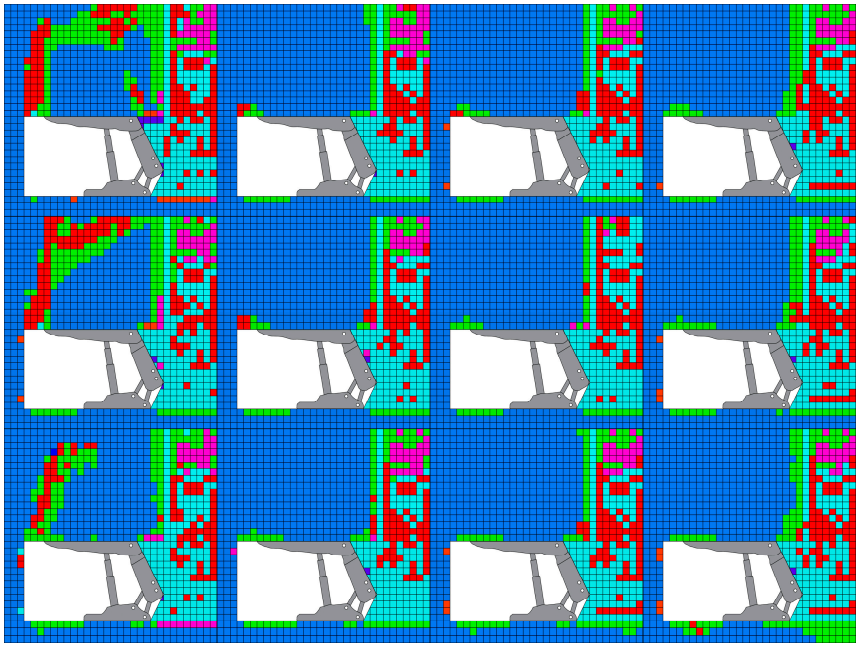			
200 m				
300 m				

The total shield convergent also reduces when compared to prior adopting the countermeasure (Figure 12). The shield convergence for the longwall face during the before web period can be seen to slightly reduce around 3% to 5%. During this period, face-to-tip distance is relatively small in both cases prior and subsequent to the adopting of the proposed countermeasure. As a result, this slight reduction of shield convergence is expected. A significant reduction can be found after web, where face-to-tip distance is relatively larger. Shield convergence during this stage reduces on average about 17%, 15%, and 4% for the depth of 100 m, 200 m, and 300 m, respectively. This indicates that shield convergence is more sensitive to the strength of the roof as higher reduction can be achieved in shallower depths where the rock is relatively weaker.

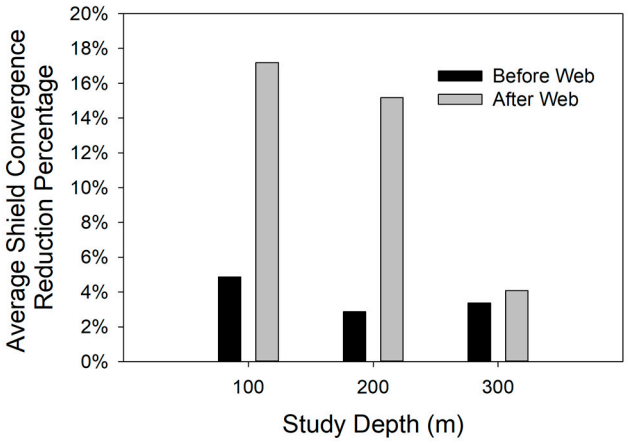

Figure 12. Average shield convergence reduction rate after adopting the countermeasure.

6. Conclusions

This research has given an account of predicting the stability of the longwall face under weak geological conditions by means of numerical analysis. The model test was

conducted under various influences including canopy ratio, shield resistance force as well as stress ratio. The outcome confirmed that the aforementioned parameters have significant influence on the stability of the longwall face which can be used for optimizing its stability. The study focuses on the failure zone and shield convergence of the face. The overall evidence from the study suggests that the biggest problem when developing longwall mining in weak geological conditions is the risk of roof fall in the longwall face.

- In weak rock, shield canopy ratio value is preferred to be nearby to 2. Shield setting pressure at the beginning of the loading cycle can be set as low as 6000 kN and after web higher shield resistance force provides better roof condition.
- The influence of the stress ratio on the roof failure zone is significant. The propagation of the failure zone above the roof of the longwall face decreases when the stress ratio increases, as the increase of horizontal stress in higher stress ratio could help counteract roof caving. However, from stress ratio 2, the horizontal failure zone starts to increase which is plausible to promote the vertical failure zone especially for weaker roofs due to excessively horizontal stress. In the lower stress ratio of 0.5, the roof caving behavior is following the detached block model. However, when the stress ratio is 1 or above, the roof caving behavior in the longwall face is following the bulking model concept.
- Shield convergence decreases following the increase of shield resistance force. The same can be said when stress ratio increases. The increment of convergence between before and after web increases in correlation with the increase of roof rock strength.

The recommended countermeasure by reducing both face-to-tip distance and cutting width shows a great effect on the stability of the longwall face. The roof failure zone for the stress ratio 1 or higher has been reduced to the allowable range which implies an excellent roof condition. However, an extra precaution in roof control is required when the stress ratio is 0.5 as a high risk of roof fall is expected. The suggested selection criteria for longwall face shield support in this weak geological condition is considering shield support capacity at least 10,000 kN, set-to-yield convergence at least 60 mm, face-to-tip distance of 0.25 m, and cutting width of 0.5 m. For future works, it is recommended to focus on roof stability under low stress ratio as well as roof shield support performant during the actual longwall operation when field monitoring of the shield support pressure and convergence are available.

Author Contributions: Conceptualization, P.M., T.S. and H.S.; methodology, P.M. and H.H.; software, P.M. and H.H.; validation, P.M., T.S. and J.O.; formal analysis, P.M., H.H. and A.H.; investigation, P.M., H.H., T.S. and Z.W.; resources, T.S., H.S., A.H. and J.O.; data curation, P.M. and T.S.; writing—original draft preparation, P.M.; writing—review and editing, P.M., T.S., Z.W. and A.H.; visualization, P.M.; supervision, T.S., H.S. and Z.W.; project administration, P.M. and A.H.; funding acquisition, T.S., H.S. and A.H. All authors have read and agreed to the published version of the manuscript.

Funding: This research received no external funding.

Institutional Review Board Statement: Not applicable.

Informed Consent Statement: Not applicable.

Acknowledgments: The authors would like to express their sincere gratitude to AUN/SEED-Net Project of JICA for providing financial support for this research.

Conflicts of Interest: The authors declare no conflict of interest.

References

1. Aydin, G. The modeling and projection of primary energy consumption by the sources. *Energy Sources Part B Econ. Plan. Policy* **2015**, *10*, 67–74. [CrossRef]
2. Azadeh, A.; Tarverdian, S. Integration of genetic algorithm, computer simulation and design of experiments for forecasting electrical energy consumption. *Energy Policy* **2007**, *35*, 5229–5241. [CrossRef]
3. Aydin, G.; Karakurt, I.; Aydiner, K. Analysis and mitigation opportunities of methane emissions from the energy sector. *Energy Sources Part A Recovery Util. Environ. Eff.* **2012**, *34*, 967–982. [CrossRef]

4. Aydin, G. The Application of trend analysis for coal demand modeling. *Energy Sources Part B Econ. Plan. Policy* **2015**, *10*, 183–191. [CrossRef]
5. Peng, S.S. Longwall mine design. In *Longwall Mining*, 3rd ed.; CRC Press: Boca Raton, FL, USA, 2019.
6. Prusek, S.; Rajwa, S.; Wrana, A.; Krzemień, A. Assessment of roof fall risk in longwall coal mines. *Int. J. Min. Reclam. Environ.* **2017**, *31*, 558–574. [CrossRef]
7. Frith, R.C. A holistic examination of the load rating design of longwall shields after more than half a century of mechanised longwall mining. *Int. J. Min. Sci. Technol.* **2015**, *25*, 687–706. [CrossRef]
8. Ji, S.; He, H.; Karlovšek, J. Application of superposition method to study the mechanical behaviour of overlying strata in longwall mining. *Int. J. Rock Mech. Min. Sci.* **2021**, *146*, 104874. [CrossRef]
9. Tian, M.; Han, L.; Xiao, H.; Meng, Q. Experimental study of deformations and failures of the coal wall in a longwall working face. *Eng. Fail. Anal.* **2021**, *125*, 105428. [CrossRef]
10. Rajwa, S.; Janoszek, T.; Prusek, S. Model tests of the effect of active roof support on the working stability of a longwall. *Comput. Geotech.* **2020**, *118*, 103302. [CrossRef]
11. Rajwa, S.; Janoszek, T.; Prusek, S. Influence of canopy ratio of powered roof support on longwall working stability—A case study. *Int. J. Min. Sci. Technol.* **2019**, *29*, 591–598. [CrossRef]
12. Zhao, T.; Liu, C.; Yetilmezsoy, K.; Gong, P.; Chen, D.; Yi, K. Segmental adjustment of hydraulic support setting load in hard and thick coal wall weakening: A study of numerical simulation and field measurement. *J. Geophys. Eng.* **2018**, *15*, 2481–2491. [CrossRef]
13. Song, G.; Chugh, Y. 3D analysis of longwall face stability in thick coal seams. *J. South. Afr. Inst. Min. Metall.* **2018**, *118*, 131–142. [CrossRef]
14. Chuang, L.; Huamin, L.; Dongjie, J. Numerical simulation study on the relationship between mining heights and shield resistance in longwall panel. *Int. J. Min. Sci. Technol.* **2017**, *27*, 293–297. [CrossRef]
15. Lv, J.; Wan, Z.; Yang, Y.; Wang, J.; Zhang, Y.; Liu, S. Failure characteristics and stability control technology of dynamic pressure roadway affected by the mining activity: A case study. *Eng. Fail. Anal.* **2022**, *131*, 105857. [CrossRef]
16. Ta, X.; Wan, Z.; Zhang, Y.; Shi, P.; Wei, Z.; Sun, X.; Jia, L. Field and Numerical Investigation on the Coal Pillar Instability of Gob-Side Entry in Gently Inclined Coal Seam. *Adv. Civ. Eng.* **2021**, *2021*, 4901670. [CrossRef]
17. Barczak, T.M. Research developments that contributed to the landscape of longwall roof support design over the past 25 years. In *Advances in Coal Mine Ground Control*; Peng, S.S., Ed.; Elsevier: Amsterdam, The Netherlands, 2017; pp. 1–34.
18. Wang, J.; Li, Y. Thick seam coal mining and its ground control. In *Advances in Coal Mine Ground Control*; Elsevier: Amsterdam, The Netherlands, 2017; pp. 379–407.
19. Witek, M.; Prusek, S. Numerical calculations of shield support stress based on laboratory test results. *Comput. Geotech.* **2016**, *72*, 74–88. [CrossRef]
20. Sasaoka, T.; Takamoto, H.; Shimada, H.; Oya, J.; Hamanaka, A.; Matsui, K. Surface subsidence due to underground mining operation under weak geological condition in Indonesia. *J. Rock Mech. Geotech. Eng.* **2015**, *7*, 337–344. [CrossRef]
21. Pongpanya, P. *Appropriate Design of Longwall Coal Mining System under Weak Geological Conditions in Indonesia*; Kyushu University: Fukuoka, Japan, 2018.
22. Mao, P.; Shimada, H.; Hamanaka, A.; Wahyudi, S.; Oya, J.; Naung, N. Three-Dimensional Analysis of Gate-Entry Stability in Multiple Seams Longwall Coal Mine Under Weak Rock Conditions. *Earth Sci. Res.* **2020**, *9*, 1–72. [CrossRef]
23. Pongpanya, P.; Sasaoka, T.; Shimada, H.; Hamanaka, A.; Wahyudi, S. Numerical Study on Effect of Longwall Mining on Stability of Main Roadway under Weak Ground Conditions in Indonesia. *J. Geol. Resour. Eng.* **2017**, *3*, 93–104. [CrossRef]
24. Pongpanya, P.; Sasaoka, T.; Shimada, H.; Ulaankhuu, B.; Oya, J.; Dwiki, S.; Karian, T. Numerical Study on Roadway Stability under Weak Geological Condition of PT Gerbang Daya Mandiri Underground Coal Mine in Indonesia. *J. Geol. Sci.* **2017**, *3*. [CrossRef]
25. Sasaoka, T.; Mao, P.; Shimada, H.; Hamanaka, A.; Oya, J. Numerical Analysis of Longwall Gate-Entry Stability under Weak Geological Condition: A Case Study of an Indonesian Coal Mine. *Energies* **2020**, *13*, 4710. [CrossRef]
26. Molinda, G.; Mark, C. Ground failures in coal mines with weak roof. *Electron. J. Geotech. Eng.* **2010**, *15*, 547–588.
27. Zhou, G.; Zhao, Z.; Song, Z.; Wang, H. Stability Analysis and Protection Measures of Large Section Tunnel in Coal Rich Weak Rock Stratum. *Geofluids* **2021**, *2021*, 1–15. [CrossRef]
28. Ghasemi, E.; Ataei, M.; Shahriar, K.; Sereshki, F.; Jalali, S.E.; Ramazanzadeh, A. Assessment of roof fall risk during retreat mining in room and pillar coal mines. *Int. J. Rock Mech. Min. Sci.* **2012**, *54*, 80–89. [CrossRef]
29. Guney, A.; Gul, M. Analysis of surface subsidence due to longwall mining under weak geological conditions: Turgut basin of Yatağan-Muğla (Turkey) case study. *Int. J. Min. Reclam. Environ.* **2019**, *33*, 445–461. [CrossRef]
30. Matsui, K.; Shimada, H.; Furukawa, H.; Kramadibrata, S.; Anwar, H. Ground control problems and roadheader drivage at Ombilin coal mine, Indonesia. In Proceedings of the 18th International Mining Congress and Exhibition of Turkey-IMCET, Antalya, Turkey, 10–13 June 2003; pp. 99–104.
31. Sasaoka, T.; Shimada, H.; Lin, N.Z.; Takamoto, H.; Matsui, K.; Kramadibrata, S.; Sulistianto, B. Geotechnical issues in the application of rock bolting technology for the development of underground coal mines in Indonesia. *Int. J. Min. Reclam. Environ.* **2014**, *28*, 150–172. [CrossRef]

32. Sasaoka, T.; Hamanaka, A.; Shimada, H.; Matsui, K.; Lin, N.Z.; Sulistianto, B. Punch multi-slice longwall mining system for thick coal seam under weak geological conditions. *J. Geol. Resour. Eng.* **2015**, *1*, 28–36. [CrossRef]
33. Garcia, A.; Altounyan, P.; Nitaramorn, A.; Lewis, A. Ground control aspects of a successful underground coal mine trial in weak strata in Indonesia. In Proceedings of the 29th International Conference on Ground Control in Mining, Morgantown, WV, USA, 27–29 June 2010; pp. 1–9.
34. Zhang, P.; Gearhart, D.; Dyke, M.V.; Su, D.; Esterhuizen, E.; Tulu, B. Ground response to high horizontal stresses during longwall retreat and its implications for longwall headgate support. *Int. J. Min. Sci. Technol.* **2019**, *29*, 27–33. [CrossRef] [PubMed]
35. Wang, F.; Zhang, C.; Zhang, X.; Song, Q. Overlying strata movement rules and safety mining technology for the shallow depth seam proximity beneath a room mining goaf. *Int. J. Min. Sci. Technol.* **2015**, *25*, 139–143. [CrossRef]
36. Anderson, T. A comparison of shallow and deep mining. In Proceedings of the Deep Mining 2014: Proceedings of the Seventh International Conference on Deep and High Stress Mining, Sudbury, ON, Canada, 16–18 September 2014; pp. 181–187.
37. Esterhuizen, G.S.; Tulu, I.B.; Gearhart, D.F.; Dougherty, H.; Van Dyke, M. Assessing support alternatives for longwall gateroads subject to changing stress. *Int. J. Min. Sci. Technol.* **2021**, *31*, 103–110. [CrossRef]
38. Stanford, C.E. Coal Resources, Production and Use in Indonesia. In *The Coal Handbook: Towards Cleaner Production*; Osborne, D., Ed.; Woodhead Publishing: Sawston, UK, 2013; Volume 2, pp. 200–219.
39. Widodo, S.; Oschmann, W.; Bechtel, A.; Sachsenhofer, R.F.; Anggayana, K.; Puettmann, W. Distribution of sulfur and pyrite in coal seams from Kutai Basin (East Kalimantan, Indonesia): Implications for paleoenvironmental conditions. *Int. J. Coal Geol.* **2010**, *81*, 151–162. [CrossRef]
40. Ngueyep Mambou, L.L.; Ndop, J.; Ndjaka, J.M.B. Numerical investigations of stresses and strains redistribution around the tunnel: Influence of transverse isotropic behavior of granitic rock, in situ stress and shape of tunnel. *J. Min. Sci.* **2015**, *51*, 497–505. [CrossRef]
41. Alehossein, H.; Poulsen, B.A. Stress analysis of longwall top coal caving. *Int. J. Rock Mech. Min. Sci.* **2010**, *47*, 30–41. [CrossRef]
42. Yavuz, H. An estimation method for cover pressure re-establishment distance and pressure distribution in the goaf of longwall coal mines. *Int. J. Rock Mech. Min. Sci.* **2004**, *41*, 193–205. [CrossRef]
43. Cheng, Y.; Wang, J.; Xie, G.; Wei, W. Three-dimensional analysis of coal barrier pillars in tailgate area adjacent to the fully mechanized top caving mining face. *Int. J. Rock Mech. Min. Sci.* **2010**, *47*, 1372–1383. [CrossRef]
44. Itasca Consulting Group Inc. *Fast Lagrangian Analysis of Continua in Three-Dimensions Manual, Ver. 5.0*; Itasca: Minneapolis, MN, USA, 2012.
45. Medhurst, T.; Hatherly, P.; Hoyer, D. Investigation of the relationship between strata characteristics and longwall caving behaviour. In Proceedings of the 14th Coal Operators Conference, University of Wollongong, Wollongong, Australia, 12–14 February 2014; pp. 51–62.
46. Cheng, J.; Peng, S.S. Study on the factors influencing the load capacity of shield. In *Advances in Coal Mine Ground Control*; Peng, S.S., Ed.; Elsevier: Amsterdam, The Netherlands, 2017; pp. 35–65.
47. Galvin, J.M. Longwall Mining. In *Ground Engineering-Principles and Practices for Underground Coal Mining*; Galvin, J.M., Ed.; Springer: Berlin, Germany, 2016.